

## Article

# Transferring A4 Paper to FeNi<sub>3</sub>/NiC<sub>x</sub> Coated Carbon Skeleton for Efficient Absorption of Multiband Microwave

Jian Wang <sup>1,†</sup>, Pengfei Yin <sup>1,\*</sup>, Junchi Liu <sup>1</sup>, Tao Zhang <sup>1</sup>, Shusheng Wang <sup>1</sup> and Lei Liu <sup>2</sup>

<sup>1</sup> College of Science, Sichuan Agricultural University, Ya'an 625014, China; wjwj8@163.com (J.W.); Liujunchi2022@163.com (J.L.); ZT1796315196@163.com (T.Z.); wangshusheng1984@163.com (S.W.)

<sup>2</sup> Department of Mechanical Engineering, Hunan University of Technology, Zhuzhou 412007, China; liulei-tyr@163.com

\* Correspondence: yinpengfei@sicau.edu.cn

† These authors contributed equally to this work.

**Abstract:** Herein, A4 typing paper was used as a novel source to manufacture FeNi<sub>3</sub> and NiC<sub>x</sub> coated carbon skeleton via facile routes. The product was examined for its ability to absorb electromagnetic emission which can be a health hazard. The impact of precursor concentration on the final electromagnetic wave absorption of samples was evaluated; the composite prepared under suitable concentration possesses outstanding multiband absorption ability of −34.64 dB and −26.7 dB at 2.32 GHz and 17.2 GHz, respectively, together with an ultra-wide effective absorption bandwidth of 9.58 GHz at only 3.9 mm. The strong dipole polarization and broad frequency range of preferable impedance matching, along with the coupling of other auxiliary mechanisms, are responsible for this excellent property. The as-prepared absorber has great potency for multiband absorption of electromagnetic waves.

**Keywords:** microwave absorption; multiband; dipole polarization; impedance matching; A4 typing paper



**Citation:** Wang, J.; Yin, P.; Liu, J.; Zhang, T.; Wang, S.; Liu, L.

Transferring A4 Paper to FeNi<sub>3</sub>/NiC<sub>x</sub> Coated Carbon Skeleton for Efficient Absorption of Multiband Microwave. *Metals* **2022**, *12*, 848. <https://doi.org/10.3390/met12050848>

Academic Editor:  
Andreas Chrysanthou

Received: 13 April 2022

Accepted: 14 May 2022

Published: 16 May 2022

**Publisher's Note:** MDPI stays neutral with regard to jurisdictional claims in published maps and institutional affiliations.



**Copyright:** © 2022 by the authors. Licensee MDPI, Basel, Switzerland. This article is an open access article distributed under the terms and conditions of the Creative Commons Attribution (CC BY) license (<https://creativecommons.org/licenses/by/4.0/>).

## 1. Introduction

Nowadays, due to the rapid development of technology in electronic information, various radio-frequency equipment has sprung up in our daily lives, resulting in the superfluous usage of electromagnetic waves (EMWs) and leading to great harm regarding electromagnetic interference (EMI) of precise instruments and to human health [1–3]. In order to overcome such problems, a great number of absorbers have been developed to eliminate the energy of EMWs by transferring it to other energies for dissipation [4–6]. In general, the ideal EMWs absorber should meet the demands of broad effective absorption bandwidth (EAB), strong absorbing ability, low density and filmy thickness [7]. Thus, the relevant troubles caused by excessive microwave radiation could be solved by these absorbers.

Up to now, numerous components of familiar materials have been utilized to absorb microwaves to some extent, such as carbon materials [8–10], ferrites [11,12], magnetic alloys [13,14], metal sulfides [15] and so on. As it is known that the microwave dissipation capacity of onefold components is relatively limited in its monotonous absorbing mechanism e.g., sole dielectric or magnetic loss, there is currently consensus that the combination of different absorbing mechanisms is necessary to strengthen the electromagnetic absorbing ability of composites [16–18]. Based on this, Zhao et al. [19] obtained core-shell Ni-Cu alloy with minimal reflection loss of −31.13 dB and EAB of 3.4 GHz for a thickness of 1.5 mm. The polarization generated from the heterogeneous structure, together with the magnetic property, of the alloy promotes electromagnetic damping capacity of microwaves. Wu et al. [20] synthesized a sandwich-like Fe<sub>3</sub>O<sub>4</sub>/Fe<sub>3</sub>S<sub>4</sub> composite with broad EAB of 5.03 GHz for 2 mm, which, owing to its unique microstructure, can endow excellent interface polarization,

as well as conduction loss to this composite. Xie et al. [21] prepared a type of carbon coated Co/CoO nanoparticle with core-shell structure; here, the porosity of the hybrid greatly increases its surface area, enhancing the interfacial polarization ability for microwave absorption. Furthermore, many investigations have employed carbon components to provide sufficient dielectric loss, regulate impedance matching and reduce the final density of composites, e.g., Hekmatara et al. [22] investigated the electromagnetic wave absorbing performance of Fe<sub>3</sub>O<sub>4</sub> modified MWCNTs, which were prepared via the typical wet chemical method. They discovered that the alignment of MWCNT/Fe<sub>3</sub>O<sub>4</sub> parallel to incident electric vector showed an enhancement of microwave absorption. Xiao et al. [23] obtained ultra-small Co/CNTs nanocomposites from the pyrolysis of a ZIF-67-based precursor, which showed excellent performance in electromagnetic absorption with maximal reflection loss (RL) of −49.16 dB at 2.5 mm. Zhou et al. [24] adjusted the content of Ni and NiO to correct the impedance matching of Ni/NiO@porous carbon composites, and achieved wide EAB of 5.12 GHz at 2.7 mm and minimum reflection loss of −51.1 dB for 2.4 mm; the porous carbon served as reductant to restore magnetic ions and offered commendable dipolar polarization loss. Hou et al. [25] prepared a biomass-derived CoFe<sub>2</sub>O<sub>4</sub>/C/PANI hierarchical composite with super-wide EAB of 8.88 GHz at 2.5 mm, this also attributed enhanced polarization loss and multiple scattering. In addition, beyond the purpose of excellent performance in absorbers, the economic and high-efficiency routes to prepare microwave absorbing materials (MAMs) still have enough significance for the obtaining of such carbon-based absorbents.

Consequently, herein a novel selection of A4 paper was transformed to carbon skeleton for loading of magnetic NPs via a facile hydrothermal-calcination route. By regulating the concentration of precursors, the electromagnetic parameters of composites could be adjusted to achieve better impedance matching in broad band, and the ultra-wide absorbing of microwave in multiple bands could also be observed, proving its practicability in electromagnetic absorption to solve the problem of superfluous microwave radiation.

## 2. Experiments

### 2.1. Reagents

Analytical nickel nitrate hexahydrate (Ni(NO<sub>3</sub>)<sub>2</sub>·6H<sub>2</sub>O), ferrous sulfate heptahydrate (FeSO<sub>4</sub>·7H<sub>2</sub>O) and urea (NH<sub>2</sub>CSNH<sub>2</sub>) were purchased from Chengdu Cologne Company, Chengdu, China. All reagents mentioned above were put to use without any purification.

### 2.2. Preparation of C@(FeNi<sub>3</sub>/NiC<sub>x</sub>) Composites

As displayed in Figure 1, the C@(FeNi<sub>3</sub>/NiC<sub>x</sub>) composites can be successfully obtained via a simple co-hydrothermal and vacuum calcination method. In a typical process, 0.834 g FeSO<sub>4</sub>·7H<sub>2</sub>O (3 mmol), 2.61 g Ni(NO<sub>3</sub>)<sub>2</sub>·6H<sub>2</sub>O (9 mmol) and 2.16 g urea (36 mmol) were consecutively dispersed in 210 mL distilled water, followed by ultrasonic dispersion for 20 mins to get homogeneous solution. Afterwards, a piece of common A4 paper was cut into two halves and folded along the longer side. Then, the folded paper was immersed in the solution and poured into a 300 mL reaction autoclave for a hydrothermal process of 140 °C/16 h. After reaction, the particle-loaded paper was washed with distilled water and dried at 70 °C, which presented a yellow-green color. Finally, it was further calcined to obtain the final product C1 at 500 °C for 2 h with a heating rate of 2 °C/min under vacuum conditions. By adjusting the additional content of FeSO<sub>4</sub>·7H<sub>2</sub>O, Ni(NO<sub>3</sub>)<sub>2</sub>·6H<sub>2</sub>O and urea to 6/9/12 mmol, 18/27/36 mmol and 72/144/288 mmol, respectively, the powders obtained were marked as C2, C3, C4 for convenient description in the following sections.

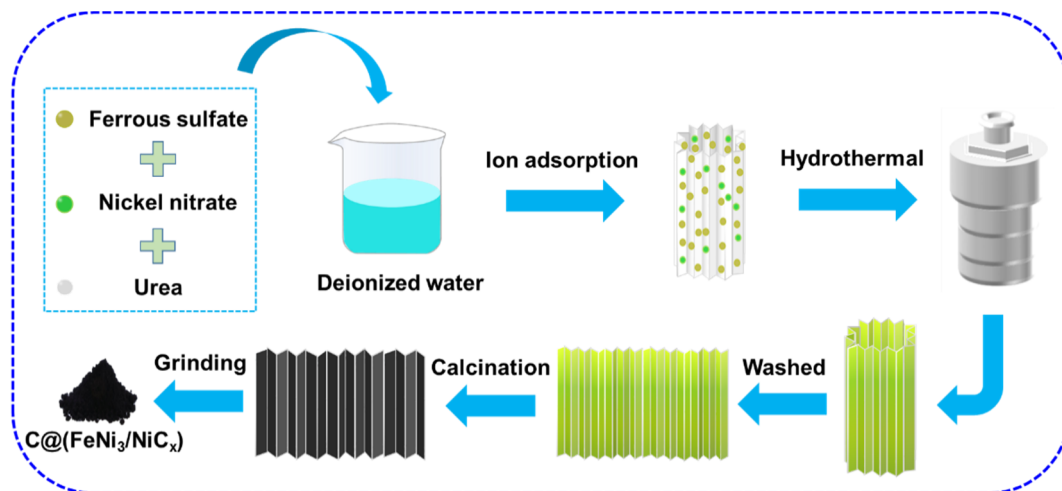


Figure 1. Synthetic route of C@(FeNi<sub>3</sub>/NiC<sub>x</sub>) composites.

### 2.3. Characterization

The crystal phases were examined by X-Ray Diffraction (XRD, D8 ADVANCE X-ray diffractometer, Bruker, Billerica, MA, USA), and the degrees of defect and graphitization in the samples were measured by Raman spectrum with 532 nm excitation wavelength (InVia Reflex, Renishaw, UK). Furthermore, transmission electron microscopy (TEM, Tecnai G2 F30, FEI, Holland) and scanning electron microscopy (SEM, SU 8010, Hitachi, Japan) were used to record the morphologies, selected area electron diffraction (SAED) and element mapping of the composites. Finally, 40 wt.% of the obtained powders were severally blended with paraffin and unfirmly pressed into ring shapes with 2 mm thickness, 3.04 mm inner diameter and 7 mm outer diameter, respectively. After that, by making use of the coaxial transmission reflection method, the electromagnetic parameter of the samples could be measured by a vector network analyzer (VNA, E5063A, Agilent, Santa Clara, CA, USA). Then, based on the transmission line theory, the RL of hybrids, representing their microwave absorbing ability, could be calculated as follows [26–28]:

$$Z_{in} = Z_0 \sqrt{\frac{\mu_r}{\epsilon_r}} \tanh\left(j \frac{2\pi f d}{c} \sqrt{\mu_r \epsilon_r}\right) \quad (1)$$

$$RL = 20 \log \left| \frac{Z_{in} - Z_0}{Z_{in} + Z_0} \right| \quad (2)$$

Here,  $Z_0$ ,  $\epsilon_r$ ,  $\mu_r$ ,  $f$ ,  $d$  and  $c$  are the impedance in air, permittivity, permeability, frequency, absorber thickness and light velocity in vacuum, respectively.

### 3. Results and Discussion

Figure 2a displays XRD curves of as-prepared C1-C4 composites. It obviously shows three peaks at 44.3°, 51.5° and 75.9°, assigned to the (111), (200) and (220) planes of FeNi<sub>3</sub> (PDF#38-0419). The formation of the alloy phase in the composites is due to high temperature reduction of carbon [29]. While the remaining peaks at 29.4°, 36.2°, 39.9°, 43.2°, 47.7° and 48.6° are generated from (111), (114), (204), (205), (123) and (009) planes of NiC<sub>x</sub> (PDF#45-0979), owing to reaction between the excess nickel source and the carbon component. No evident peaks for graphitized carbon can be observed in the composites, which means the carbon component here may be in an amorphous state. Figure 2b displays the Raman spectrum of these composites, with typical peaks around 1580 cm<sup>-1</sup> and 1340 cm<sup>-1</sup> are in G and D bands, respectively. The D band is related to disordered carbon atoms e.g., defects, groups and grain boundaries etc., and the G band is generated from the vibration of carbon atoms in plane, indicating the graphitization of carbon atoms [30,31]. It shows that the D and G peaks wear off gradually from C1 to C4, owing to the increasing

concentration of Fe and Ni sources in the precursor for the preparation of such composites, resulting in reduction of carbon content in the final products. However, the strength ratios of D to G peaks are 0.78, 0.81, 0.89 and 0.97, respectively; the increasing tendency indicates more disorders can be acted on as sites of dipole polarization to strengthen the dielectric loss of the C4 sample [32].

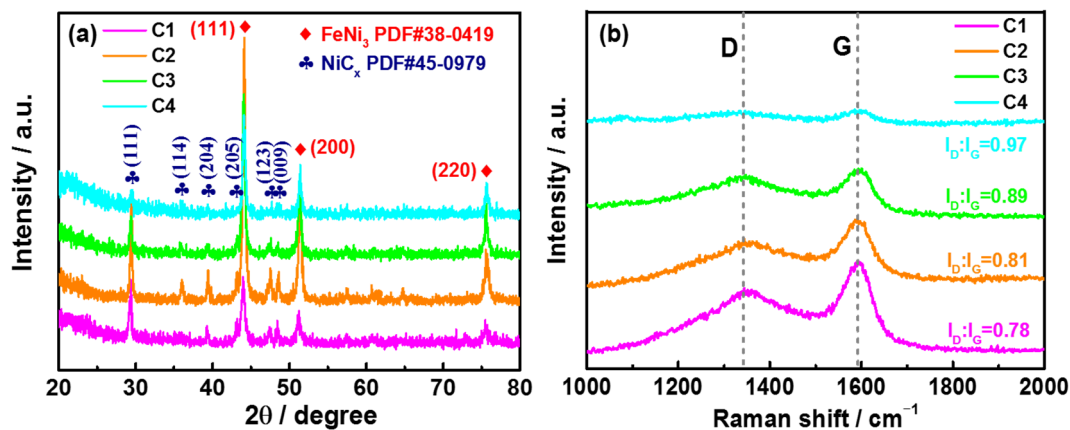
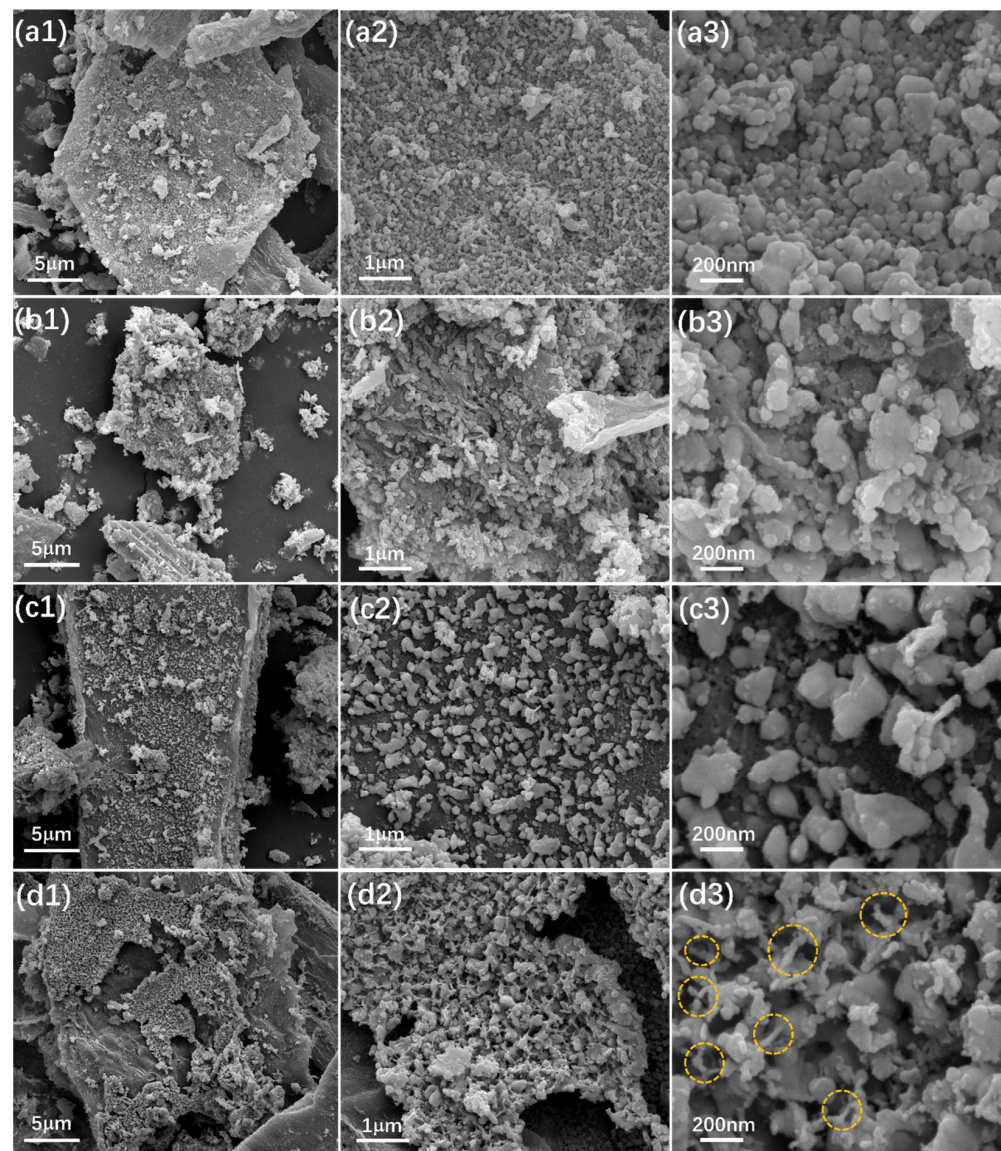


Figure 2. XRD curves (a) and Raman spectrum (b) of C1–C4 composites.

The SEM images of C1–C4 composites are shown in Figure 3. They indicate that the morphology of C1 presents laminated sheets with plentiful NPs bonded uniformly on the surface. In Figure 3(b1–b3), it can be seen that the aggregation of bonded NPs seems to become larger and some are embedded in the crack of the sheets. Nevertheless, the aggregations that adhered on the surface appear in a state of scattered distribution in the C3 sample. This dispersive aggregation would further stick together and form a large area of loose structure with tiny filar particles implanted, as displayed in Figure 3(d3). The porosity of the C4 sample is conducive to the multiple scattering loss of electromagnetic waves and the reduction of density in the composite [33,34].

Here, the above C4 composite was selected as the typical case to be further observed via the TEM technique. In Figure 4a, the formed NPs are all adhered to the laminated skeleton, which is made up of amorphous carbon, as shown in Figure 4b. Moreover, Figure 4c also indicates that there is a thin carbon layer coated on the surface of these NPs, migrating from the carbon frame under the action of high temperature thermal diffusion [35]; this is an important factor to optimize impedance matching of NPs in the composite [36]. Figure 4d shows the crystal spacing of 0.204 nm in a large particle, corresponding to the (111) plane of FeNi<sub>3</sub> phase, while the spacing of 0.248 nm and 0.209 nm in small particles are (114) and (205) planes of NiC<sub>x</sub>. Besides, apart from (205) plane of NiC<sub>x</sub>, Figure 4e displays the (200) plane of FeNi<sub>3</sub> with crystal spacing of 0.177 nm as well. In addition, a large quantity of defects can be found in NiC<sub>x</sub> particles and are marked in the dotted circle, foreboding potential dipole polarization for microwave loss at these sites [37]. Figure 4f shows several diffraction rings in SAED of reciprocal space, indicating the polycrystalline property of these NPs. Furthermore, the representational points for (111) and (220) planes of FeNi<sub>3</sub> together with (114) and (205) planes of NiC<sub>x</sub> can be simultaneously observed, which is in agreement with the results of XRD. The element mapping of Figure 4g reveals that the Ni and Fe elements are located at the region of nanoparticles; however, the C element is distributed within the whole frame.



**Figure 3.** SEM images of C1 (a1–a3), C2 (b1–b3), C3 (c1–c3) and C4 (d1–d3).

Usually, the electromagnetic wave absorption effect of MAMs can be characterized by RL; a value lower than  $-10$  dB stands for absorptivity above 90% [38]. Figure 5a indicates that the maximum RL of C1 sample is  $-34.74$  dB at 10.56 GHz for a thickness of 7 mm, and the widest EAB is 5.01 GHz i.e., 3.22–4.82 GHz and 11.05–14.46 GHz at 5.69 mm. As displayed in Figure 5b, the maximal RL of the C2 sample is  $-32.42$  dB at 11.12 GHz for 6 mm. Also, decreasing thickness of 5.22 mm for broad EAB of 5.6 GHz (3.14–4.94 GHz and 11.01–14.81 GHz) can be observed. Though the absorbing intensity of the C3 sample reduces to  $-27.05$  dB at 10.72 GHz, the related thickness also decreases to 5.5 mm and the broadest EAB slightly increases to 5.72 GHz (3.02–4.7 GHz and 10.63–14.67 GHz) at 4.76 mm. It is surprising that the microwave absorbing ability of C4 composite enhances to a large extent. Figure 5d shows that the optimized RL of  $-34.64$  dB at low frequency region of 2.32 GHz can be noted for 5 mm, there is another large RL of  $-26.7$  dB at 17.2 GHz for thinner thickness of 3.5 mm as well. Moreover, the broadest EAB has been greatly improved to an ultra-wide range of 9.58 GHz (2.03–3.43 GHz, 9.37–12.96 GHz and 13.41–18 GHz) for only 3.9 mm. The additional EAB of 2.28 GHz within the frequency range of 3.48–5.76 GHz indicates its excellent absorption of low frequency microwaves at a thinner thickness of 1.58 mm. Most importantly, the electromagnetic absorption in multiband denotes the extensive utility of this composite for complicated environments of microwave radiation.

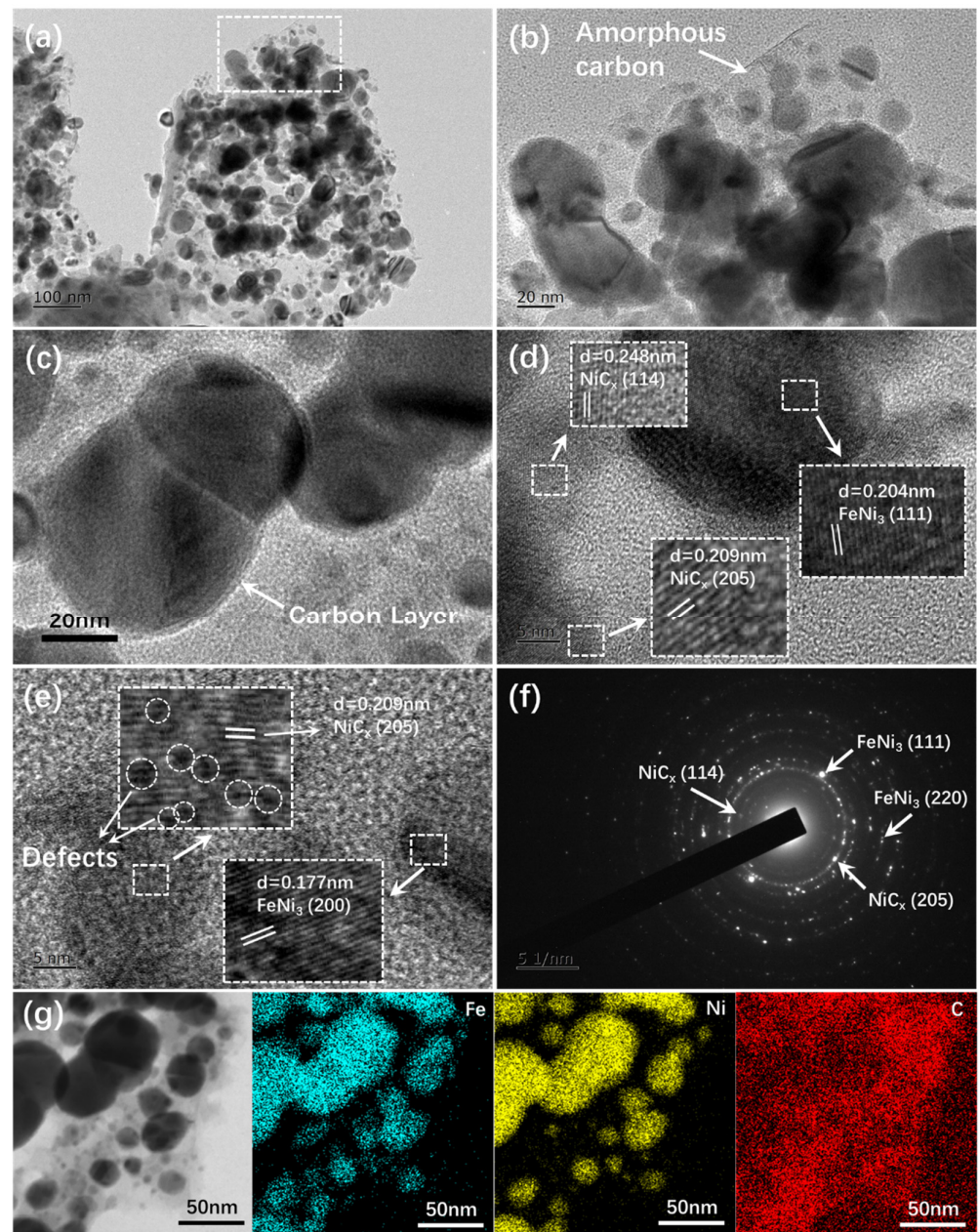


**Figure 4.** TEM images (a–c), HR-TEM images (d) and (e), SAED (f) and elements distribution (g) of C4 composite.

In general, the electromagnetic parameters of permeability ( $\mu_r = \mu_r' - j\mu_r''$ ) and permittivity ( $\epsilon_r = \epsilon_r' - j\epsilon_r''$ ) are closely related with the electromagnetic behavior and impedance matching property of the composite. Figure 6a shows the decreasing tendency of  $\epsilon_r'$  in all samples with increasing of frequency, owing to the dielectric dispersion effect of delay in polarization process [39]. The  $\epsilon_r''$  of composites presents a pattern of firstly increase and then decrease; particularly the C4 sample, which shows higher  $\epsilon_r''$  in the low frequency range, indicating that its preferable low frequency absorbing capacity is mainly due to dielectric loss, for this imaginary part means the dielectric dissipation of electromagnetic wave energy in composite [40]. Hence, the dielectric loss tangent in composites have the same change rule as the imaginary part, i.e., better dielectric tangent of C4 in lower region and weak intensity in higher range; this is consistent with its RL. Figure 6d displays the  $\mu_r'$  of C1–C4 samples and it can be seen that these first increase and then decrease for enhancement of frequency. Moreover, the  $\mu_r''$  shows a similar tendency

in Figure 6e; in which the lower values of C4 within the high frequency range indicate its weaker magnetic dissipation. Thus, the tangent angle of magnetic loss also reveals this distinction compared with the other three samples. Moreover, here the negative part of permittivity can be explained by the Drude model. The oscillation would occur under high frequency, due to the simple harmonic motion of free electrons from the alloy phase at altering electromagnetic field, as well as the mechanism of negative permeability derived from the law of electromagnetic induction, i.e., the direction of induced magnetic field is opposite to the external magnetic field, which would cancel part of the external magnetic field and thus lead to negative susceptibility [41].

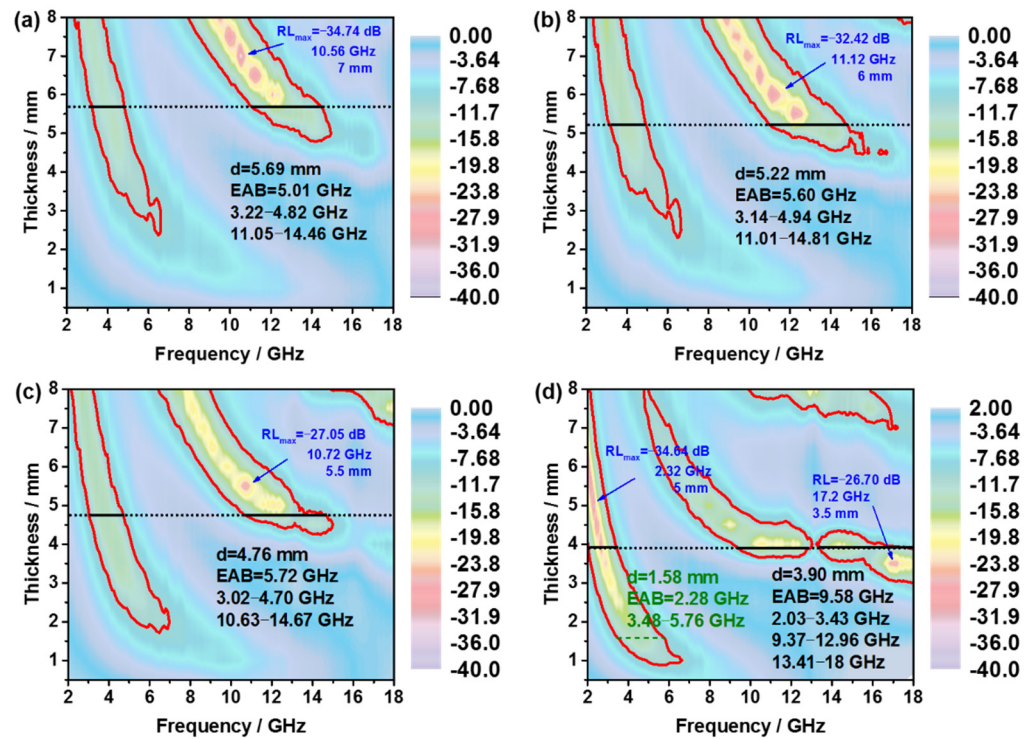


Figure 5. Electromagnetic wave reflection loss of C1 (a), C2 (b), C3 (c) and C4 (d).

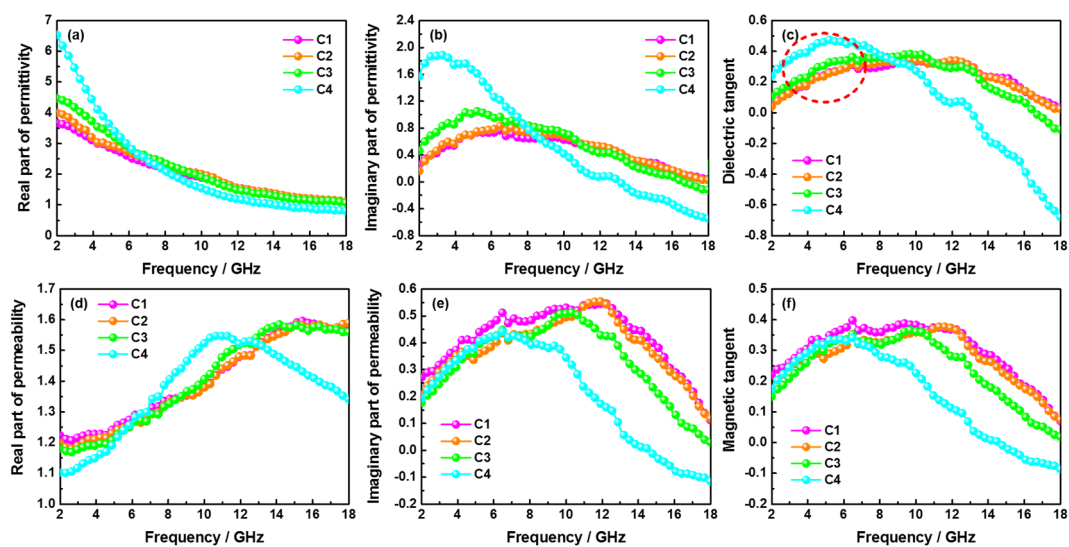


Figure 6. Permittivity (a) and (b), dielectric loss tangent (c), permeability (d) and (e), magnetic loss tangent (f) of C1–C4 composites.

In order to further evaluate the effect of interfacial polarization in dielectric loss, the Debye theory can be used to describe such polarization relaxation behavior [42,43]:

$$\varepsilon_r' = \varepsilon_\infty + \frac{\varepsilon_s - \varepsilon_\infty}{1 + (2\pi f\tau)^2} \quad (3)$$

$$\varepsilon_r'' = \frac{2\pi f\tau(\varepsilon_s - \varepsilon_\infty)}{1 + (2\pi f\tau)^2} + \frac{\sigma}{2\pi f\varepsilon_0} \quad (4)$$

where,  $\varepsilon_s$ ,  $\varepsilon_\infty$ ,  $\varepsilon_0$ ,  $\sigma$  and  $\tau$  are the static permittivity, infinite permittivity, vacuum permittivity, conductivity and relaxation time, respectively.

Based on above Equations (3) and (4), the relationship between  $\varepsilon_r'$  and  $\varepsilon_r''$  is expressed as following [44]:

$$\left(\varepsilon_r' - \frac{\varepsilon_s + \varepsilon_\infty}{2}\right)^2 + (\varepsilon_r'')^2 = \left(\frac{\varepsilon_s - \varepsilon_\infty}{2}\right)^2 \quad (5)$$

Formula (5) denotes the equation of a circle, which means one Cole-Cole semicircle represents a relaxation process of interface polarization. In Figure 7a, four semicircles can be observed in C1, suggesting the process of multiple polarization relaxation in this sample. Three obvious semicircles in C2 and C3 suggest the weakened interface polarization effect in these two samples. However, the further reduced Cole-Cole semicircles in C4 sample illustrates that the interface polarization is not the main reason for its remarkable microwave absorbing ability.

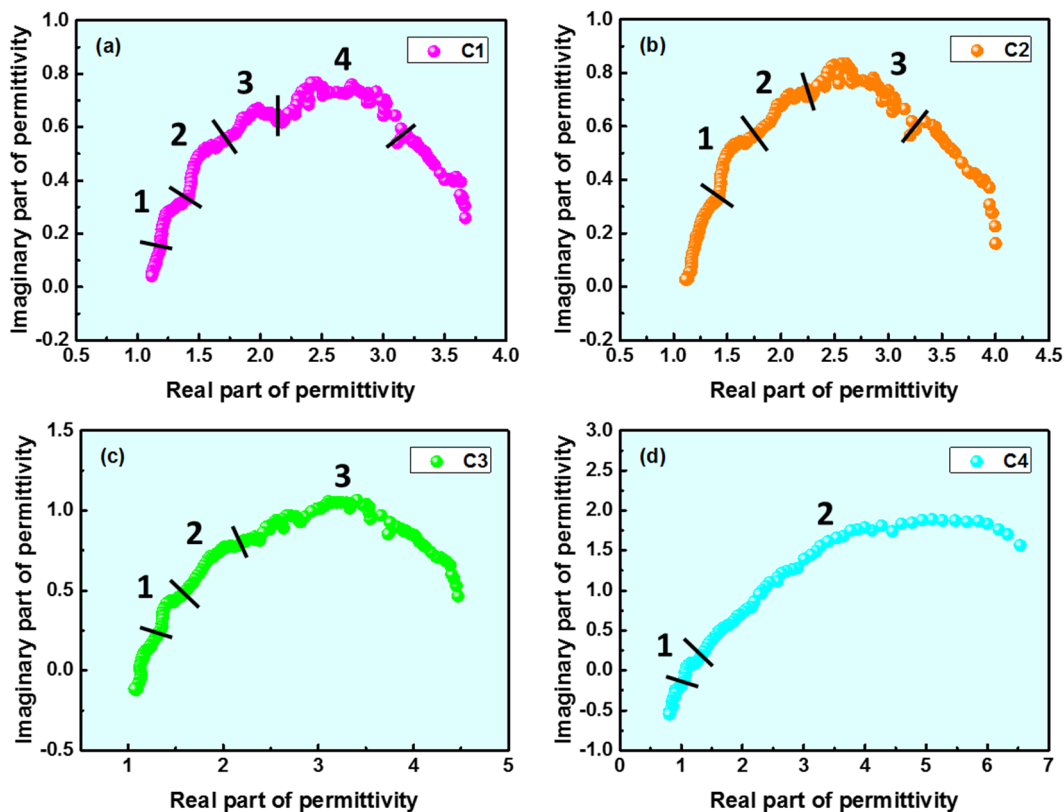


Figure 7. Cole-Cole curves of C1 (a), C2 (b), C3 (c) and C4 (d).

In terms of magnetic loss, domain-wall resonance occurs in the MHz range and the hysteresis dissipation in weak field could be neglected. The remaining exchange and nature

resonance, and eddy-current loss take play in GHz range, in which the eddy-current loss effect is characterized by the  $C_0$  parameter [45,46]:

$$C_0 = \mu_r'' (\mu_r')^{-2} f^{-1} \approx 2\pi\mu_0\sigma d^2 / 3 \quad (6)$$

The unchanged  $C_0$  forebodes the powerful eddy-current loss in the microwave absorption process. In Figure 8a, here the continuous declining of  $C_0$  in all samples indicates insignificant eddy current dissipation in these composites. The dominating absorption in C4 samples is attributed to dipole polarization produced by abundant defects as displayed in Figures 2b and 4e. Besides, the comprehensive judgment of microwave transmission capacity in absorbers could be characterized by attenuation constant ( $\alpha$ ), which is represented as following [47–49]:

$$\alpha = \frac{\sqrt{2}\pi f}{c} \times \sqrt{(\mu''\epsilon'' - \mu'\epsilon') + \sqrt{(\mu''\epsilon'' - \mu'\epsilon')^2 + (\mu'\epsilon'' + \mu''\epsilon')^2}} \quad (7)$$

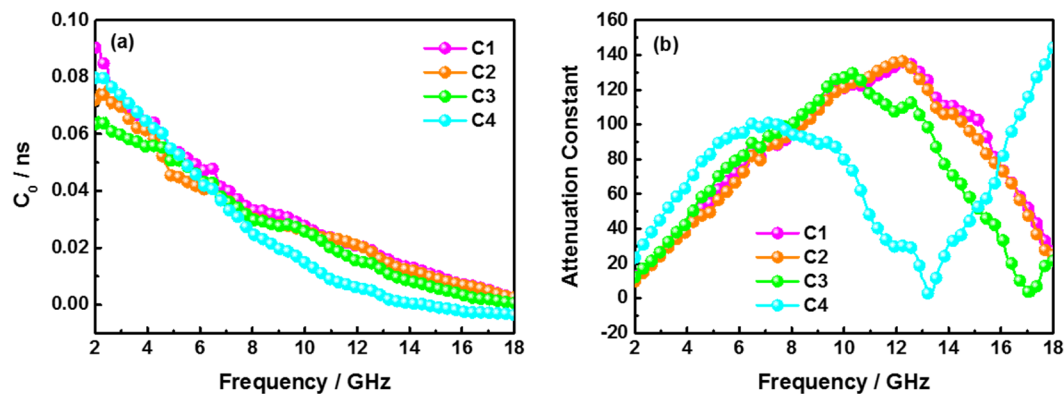


Figure 8. Parameter for eddy current effect (a) and attenuation constant (b) in C1–C4 composites.

The larger  $\alpha$  indicates a weaker transmission of microwave in composite. Figure 8b shows the  $\alpha$  of C1 and C2 are increasing first and then decreasing as frequency is enhanced, while that of C3 and C4 would re-increase again after the aforementioned damping. It can be obviously noted that the  $\alpha$  of C4 possesses larger values within the lower and higher frequency regions, which is why it has better absorption at the corresponding range.

Most importantly, impedance matching is a principal element in determining whether the incident microwave could enter into the MAMs to be further consumed [50]. Figure 9 gives the impedance distribution of C1–C4 composites under different thicknesses. The areas between two red lines of 0.8 and 1.2 are adaptive regions for acceptable matching condition. Hence, it is obvious that the multiband matching of impedance in samples promote their microwave absorption in these bands. Moreover, the reducing thickness of matched impedance from C1 to C4 suggests the realizable EAB in thinner thickness, especially the wider matching region of impedance in C4 composite provides its broad EAB compared with other samples. Figure 10 displays the comparison of electromagnetic wave absorption properties in these samples. Apparently the C4 possesses relatively large RL with super-wide EAB at thinnest thickness. Moreover, the detailed microwave absorbing performance of as-prepared C4 and other related EMW absorbers are shown in Figure 11 [5,6,9–13,51,52]. It can be seen that the EAB of C4 is much wider than that of other composites, though the thickness is 3.9 mm; indicating its wide prospect of application for practical usage.

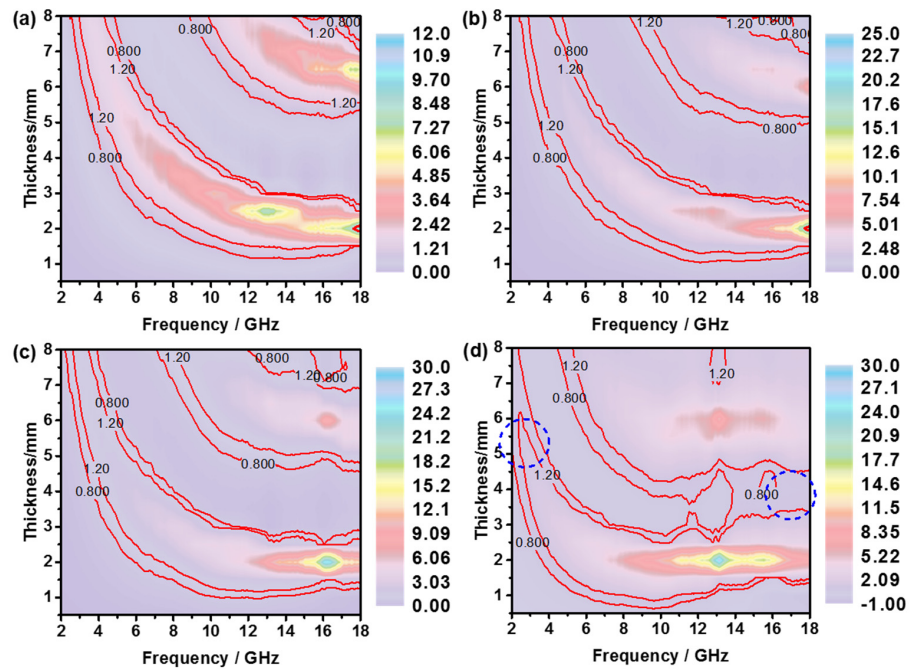


Figure 9. 2D diagram of impedance matching distribution in C1 (a), C2 (b), C3 (c) and C4 (d).

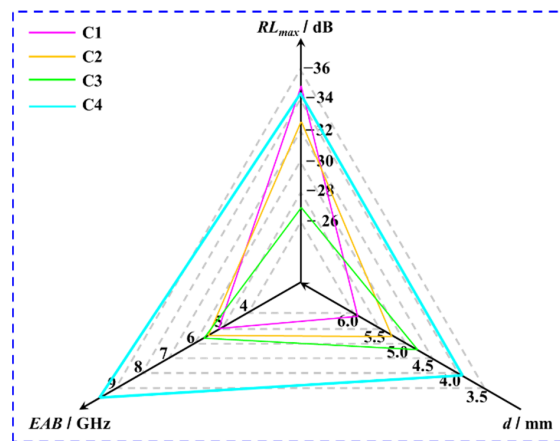


Figure 10. Comparison of electromagnetic wave absorption properties in C1–C4 composites.

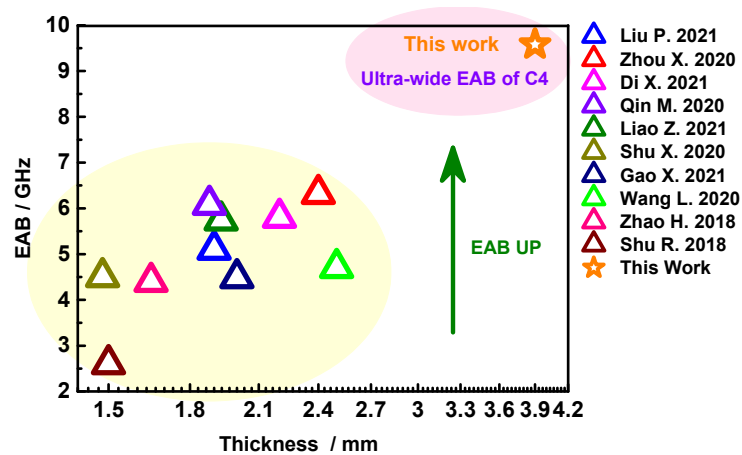


Figure 11. Microwave absorbing performance between as-prepared C4 and other composites reported in literatures.

#### 4. Conclusions

In summary, herein a novel carbon source of A4 typing paper was employed to prepare C@(FeNi<sub>3</sub>/NiC<sub>x</sub>) composite by facile hydrothermal and annealing routes. The influence of precursor concentration on morphology, electromagnetic parameters and electromagnetic wave absorbing performance of as-prepared hybrids were discussed. The C4 composite presents a multiband absorption phenomenon, which possesses the optimal RL of −34.64 dB and −26.7 dB at 2.32 GHz and 17.2 GHz, respectively. Moreover, its super-wide EAB of 9.58 GHz would be attained at only 3.9 mm. This excellent microwave absorption ability is mainly owing to the better impedance matching in broadband and powerful dipole polarization induced by abundant defects etc. Thus, the multiband absorber prepared here has an expansive application prospect.

**Author Contributions:** Writing—original draft preparation, J.W.; writing—review and editing, P.Y.; methodology, J.L.; investigation, T.Z. and S.W.; data curation, L.L. All authors have read and agreed to the published version of the manuscript.

**Funding:** This research was funded by Surface Project of Local Development in Science and Technology Guided by Central Government, grant number 2021ZYD0041; Natural Science Foundation of Hunan Province, grant number 2021JJ40175. And The APC was funded by Surface Project of Local Development in Science and Technology Guided by Central Government, grant number 2021ZYD0041.

**Institutional Review Board Statement:** Not applicable.

**Informed Consent Statement:** Not applicable.

**Data Availability Statement:** Not applicable.

**Acknowledgments:** This investigation has been supported by the Surface Project of Local Development in Science and Technology Guided by Central Government (No.2021ZYD0041) and Natural Science Foundation of Hunan Province (No.2021JJ40175).

**Conflicts of Interest:** The authors declare no conflict of interest.

#### References

1. Qin, M.; Lan, D.; Liu, J.; Liang, H.; Zhang, L.; Xing, H.; Xu, T.; Wu, H. Synthesis of single-component metal oxides with controllable multi-shelled structure and their morphology-related applications. *Chem. Rec.* **2020**, *20*, 102–119. [[CrossRef](#)] [[PubMed](#)]
2. Gao, S.; Zhang, G.; Wang, Y.; Han, X.; Huang, Y.; Liu, P. MOFs derived magnetic porous carbon1 microspheres constructed by core-shell Ni@C with high-performance microwave absorption. *J. Mater. Sci. Technol.* **2021**, *88*, 56–65. [[CrossRef](#)]
3. Wang, J.; Jia, Z.; Liu, X.; Dou, J.; Xu, B.; Wang, B.; Wu, G. Construction of 1D heterostructure NiCo@C/ZnO nanorod with enhanced microwave absorption. *Micro-Nano Lett.* **2021**, *13*, 175. [[CrossRef](#)] [[PubMed](#)]
4. Gao, Z.; Lan, D.; Zhang, L.; Wu, H. Simultaneous manipulation of interfacial and defects polarization toward Zn/Co phase and ion hybrids for electromagnetic wave absorption. *Adv. Funct. Mater.* **2021**, *31*, 2106677. [[CrossRef](#)]
5. Liu, P.; Gao, S.; Zhang, G.; Huang, Y.; You, W.; Che, R. Hollow engineering to Co@N-doped carbon nanocages via synergistic protecting-etching strategy for ultrahigh microwave absorption. *Adv. Funct. Mater.* **2021**, *31*, 2102812. [[CrossRef](#)]
6. Zhou, X.; Jia, Z.; Feng, A.; Qu, S.; Wang, X.; Liu, X.; Wang, B.; Wu, G. Synthesis of porous carbon embedded with NiCo/CoNiO<sub>2</sub> hybrids composites for excellent electromagnetic wave absorption performance. *J. Colloid. Interf. Sci.* **2020**, *575*, 130–139. [[CrossRef](#)]
7. Qin, M.; Zhang, L.; Zhao, X.; Wu, H. Lightweight Ni foam-based ultra-broadband electromagnetic wave absorber. *Adv. Funct. Mater.* **2021**, *31*, 2103436. [[CrossRef](#)]
8. Zhou, J.; Wang, M.; Shu, X.; Ma, J.; Ren, H.; Wang, Y.; Liu, Y.; Shu, R.; Oh, W.C.; Kong, L.B. Facile synthesis of La-doped cobalt ferrite@glucose-based carbon composite as effective multiband microwave absorber. *J. Am. Ceram. Soc.* **2021**, *104*, 2191–2200. [[CrossRef](#)]
9. Di, X.; Wang, Y.; Lu, Z.; Cheng, R.; Yang, L.; Wu, X. Heterostructure design of Ni/C/porous carbon nanosheet composite for enhancing the electromagnetic wave absorption. *Carbon* **2021**, *179*, 566–578. [[CrossRef](#)]
10. Qin, M.; Liang, H.; Zhao, X.; Wu, H. Filter paper templated one-dimensional NiO/NiCo<sub>2</sub>O<sub>4</sub> microrod with wideband electromagnetic wave absorption capacity. *J. Colloid Inter. Sci.* **2020**, *566*, 347–356. [[CrossRef](#)]
11. Liao, Z.; Ma, M.; Tong, Z.; Wang, R.; Bi, Y.; Chen, Y.; Chung, K.L.; Ma, Y. Fabrication of ZnFe<sub>2</sub>O<sub>4</sub>/C@PPy composites with efficient electromagnetic wave absorption properties. *J. Colloid Interf. Sci.* **2021**, *602*, 602–611. [[CrossRef](#)] [[PubMed](#)]

12. Shu, X.; Ren, H.; Jiang, Y.; Zhou, J.; Wang, Y.; Wang, Y.; Liu, Y.; Oh, W.C. Enhanced electromagnetic wave absorption performance of silane coupling agent KH550@Fe<sub>3</sub>O<sub>4</sub> hollow nanospheres/graphene composites. *J. Mater. Chem. C* **2020**, *8*, 2913–2926. [[CrossRef](#)]
13. Gao, X.; Jia, Z.; Wang, B.; Wu, X.; Sun, T.; Liu, X.; Chi, Q.; Wu, G. Synthesis of NiCo-LDH/MXene hybrids with abundant heterojunction surfaces as a lightweight electromagnetic wave absorber. *Chem. Eng. J.* **2021**, *419*, 130019. [[CrossRef](#)]
14. Yin, P.; Zhang, L.; Tang, Y.; Liu, J. Earthworm-like (Co/CoO)@C composite derived from MOF for solving the problem of low-frequency microwave radiation. *J. Alloy. Compd.* **2021**, *881*, 160556. [[CrossRef](#)]
15. Liu, J.; Zhang, L.; Zang, D.; Wu, H. A competitive reaction strategy toward binary metal sulfides for tailoring electromagnetic wave absorption. *Adv. Funct. Mater.* **2021**, *31*, 2105018. [[CrossRef](#)]
16. Huang, X.; Liu, X.; Jia, Z.; Wang, B.; Wu, X.; Wu, G. Synthesis of 3D cerium oxide/porous carbon for enhanced electromagnetic wave absorption performance. *Adv. Compos. Hybrid Mater.* **2021**, *4*, 1398–1412. [[CrossRef](#)]
17. Di, X.; Wang, Y.; Fu, Y.; Wu, X.; Wang, P. Controllable heterogeneous interfaces of cobalt/carbon nanosheets/rGO composite derived from metal-organic frameworks for high-efficiency microwave attenuation. *Carbon* **2022**, *187*, 404–414.
18. Yin, P.; Zhang, L.; Sun, P.; Wang, J.; Feng, X.; Zhang, Y.; Dai, J.; Tang, Y. Apium-derived biochar loaded with MnFe<sub>2</sub>O<sub>4</sub>@C for excellent low frequency electromagnetic wave absorption. *Ceram. Int.* **2020**, *46*, 13641–13650. [[CrossRef](#)]
19. Zhao, B.; Zhao, W.; Shao, G.; Fan, B.; Zhang, R. Morphology-control synthesis of a core-shell structured NiCu alloy with tunable electromagnetic-wave absorption capabilities. *ACS Appl. Mater. Interf.* **2015**, *7*, 12951–12960. [[CrossRef](#)]
20. Wu, H.; Liu, J.; Liang, H.; Zang, D. Sandwich-like Fe<sub>3</sub>O<sub>4</sub>/Fe<sub>3</sub>S<sub>4</sub> composites for electromagnetic wave absorption. *Chem. Eng. J.* **2020**, *393*, 124743. [[CrossRef](#)]
21. Xie, X.; Pang, Y.; Kikuchi, H.; Liu, T. The synergistic effects of the carbon coating and micropore structure on the microwave absorption properties of the Co/CoO nanoparticles. *Phys. Chem. Chem. Phys.* **2016**, *18*, 30507–30514. [[CrossRef](#)] [[PubMed](#)]
22. Hekmatara, H.; Seifi, M.; Forooghi, K. Microwave absorption property of aligned MWCNT/Fe<sub>3</sub>O<sub>4</sub>. *J. Magn. Magn. Mater.* **2013**, *346*, 186–191. [[CrossRef](#)]
23. Xiao, X.; Zhu, W.; Tan, Z.; Tian, W.; Guo, Y.; Wang, H.; Fu, J.; Jian, X. Ultra-small Co/CNTs nanohybrid from metal organic framework with highly efficient microwave absorption. *Compos. Part B* **2018**, *152*, 316–323. [[CrossRef](#)]
24. Zhou, X.; Jia, Z.; Zhang, X.; Wang, B.; Wu, W.; Liu, X.; Xu, B.; Wu, G. Controllable synthesis of Ni/NiO@porous carbon hybrid composites towards remarkable electromagnetic wave absorption and wide absorption bandwidth. *J. Mater. Sci. Technol.* **2021**, *87*, 120–132. [[CrossRef](#)]
25. Hou, T.; Jia, Z.; Feng, A.; Zhou, Z.; Liu, X.; Lv, H.; Wu, G. Hierarchical composite of biomass derived magnetic carbon framework and phytic acid doped polyaniline with prominent electromagnetic wave absorption capacity. *J. Mater. Sci. Technol.* **2021**, *68*, 61–69. [[CrossRef](#)]
26. Wang, L.; Huang, M.; Yu, X.; You, W.; Zhang, J.; Liu, X.; Wang, M.; Che, R. MOF-derived Ni<sub>1-x</sub>Co<sub>x</sub>@carbon with tunable nano-microstructure as lightweight and highly efficient electromagnetic wave absorber. *Nano-Micro Lett.* **2020**, *12*, 150. [[CrossRef](#)]
27. Zhang, F.; Jia, Z.; Wang, Z.; Zhang, C.; Wang, B.; Xu, B.; Liu, X.; Wu, G. Tailoring nanoparticles composites derived from metal-organic framework as electromagnetic wave absorber. *Mater. Today Phys.* **2021**, *20*, 100475. [[CrossRef](#)]
28. Sun, C.; Jia, Z.; Xu, S.; Hu, D.; Zhang, C.; Wu, G. Synergistic regulation of dielectric-magnetic dual-loss and triple heterointerface polarization via magnetic MXene for high-performance electromagnetic wave absorption. *J. Mater. Sci. Technol.* **2022**, *113*, 128–137. [[CrossRef](#)]
29. Ma, M.; Liao, Z.; Su, X.; Zheng, Q.; Liu, Y.; Wang, Y.; Ma, Y.; Wan, F. Magnetic CoNi alloy particles embedded N-doped carbon fibers with polypyrrole for excellent electromagnetic wave absorption. *J. Colloid Inter. Sci.* **2022**, *608*, 2203–2212. [[CrossRef](#)]
30. Cheng, R.; Wang, Y.; Di, X.; Lu, Z.; Wang, P.; Ma, M.; Ye, J. Construction of MOF-derived plum-like NiCo@C composite with enhanced multi-polarization for high-efficiency microwave absorption. *J. Colloid Inter. Sci.* **2022**, *609*, 224–234. [[CrossRef](#)]
31. Dai, B.; Zhao, B.; Xie, X.; Su, T.; Fan, B.; Zhang, R.; Yang, R. A novel two-dimensional Ti<sub>3</sub>C<sub>2</sub>T<sub>x</sub> MXenes/nano-carbon spheres hybrids for high-performance microwave absorption. *J. Mater. Chem. C* **2018**, *6*, 5690–5697. [[CrossRef](#)]
32. Liu, J.; Zhang, L.; Wu, H. Electromagnetic wave-absorbing performance of carbons, carbides, oxides, ferrites and sulfides: Review and perspective. *J. Phys. D Appl. Phys.* **2021**, *54*, 203001. [[CrossRef](#)]
33. Cao, X.; Jia, Z.; Hu, D.; Wu, G. Synergistic construction of three-dimensional conductive network and double heterointerface polarization via magnetic FeNi for broadband microwave absorption. *Adv. Compos. Hybrid Mater.* **2022**, 1–4. [[CrossRef](#)]
34. Lan, D.; Qin, M.; Yang, R.; Chen, S.; Wu, H.; Fan, Y.; Fu, Q.; Zhang, F. Facile synthesis of hierarchical chrysanthemum-like copper cobaltate-copper oxide composites for enhanced microwave absorption performance. *J. Colloid Inter. Sci.* **2019**, *533*, 481–491. [[CrossRef](#)]
35. Yin, P.; Zhang, L.; Wang, J.; Feng, X.; Zhang, Y.; Dai, J.; Liu, J. Tailoring microstructures in (Ni/NiO)@C composites via facile route for broadband microwave absorption. *Ceram. Int.* **2022**, *48*, 12979–12987. [[CrossRef](#)]
36. Hou, T.; Jia, Z.; Dong, Y.; Liu, X.; Wu, G. Layered 3D structure derived from MXene/magnetic carbon nanotubes for ultra-broadband electromagnetic wave absorption. *Chem. Eng. J.* **2022**, *431*, 133919. [[CrossRef](#)]
37. Liu, J.; Zhang, L.; Wu, H.; Zang, D. Boosted electromagnetic wave absorption performance from vacancies, defects and interfaces engineering in Co(OH)F/Zn<sub>0.76</sub>Co<sub>0.24</sub>S/Co<sub>3</sub>S<sub>4</sub> composite. *Chem. Eng. J.* **2021**, *411*, 128601. [[CrossRef](#)]
38. Hou, T.; Jia, Z.; Wang, B.; Li, H.; Liu, X.; Chi, Q.; Wu, G. Metal-organic framework derived NiSe<sub>2</sub>-CoSe<sub>2</sub>@C/Ti<sub>3</sub>C<sub>2</sub>T<sub>x</sub> composites as electromagnetic wave absorbers. *Chem. Eng. J.* **2021**, *422*, 130079. [[CrossRef](#)]

39. Liao, Z.; Ma, M.; Tong, Z.; Bi, Y.; Chung, K.L.; Qiao, M.; Ma, Y.; Ma, A.; Wu, G.; Li, Z.; et al. Fabrication of one-dimensional ZnFe<sub>2</sub>O<sub>4</sub>@carbon@MoS<sub>2</sub>/FeS<sub>2</sub> composites as electromagnetic wave absorber. *J. Colloid Interf. Sci.* **2021**, *599*, 262–270. [[CrossRef](#)]
40. Liu, Y.; Liu, X.; E, X.; Wang, B.; Jia, Z.; Chi, Q.; Wu, G. Synthesis of Mn<sub>x</sub>O<sub>y</sub>@C hybrid composites for optimal electromagnetic wave absorption capacity and wideband absorption. *J. Mater. Sci. Technol.* **2022**, *103*, 157–164. [[CrossRef](#)]
41. Xie, P.; Zhang, Z.; Wang, Z.; Sun, K.; Fan, R. Targeted double negative properties in silver/silica random metamaterials by precise control of microstructures. *Research* **2019**, *2019*, 1021368. [[CrossRef](#)] [[PubMed](#)]
42. Zhao, Z.; Kou, K.; Zhang, L.; Wu, H. Optimal particle distribution induced interfacial polarization in bouquet-like hierarchical composites for electromagnetic wave absorption. *Carbon* **2021**, *186*, 323–332. [[CrossRef](#)]
43. Chen, G.; Zhang, L.; Luo, B.; Wu, H. Optimal control of the compositions, interfaces, and defects of hollow sulfide for electromagnetic wave absorption. *J. Colloid Interf. Sci.* **2021**, *607*, 24–33. [[CrossRef](#)] [[PubMed](#)]
44. Gao, Z.; Xu, B.; Ma, M.; Feng, A.; Zhang, Y.; Liu, X.; Jia, Z.; Wu, G. Electrostatic self-assembly synthesis of ZnFe<sub>2</sub>O<sub>4</sub> quantum dots (ZnFe<sub>2</sub>O<sub>4</sub>@C) and electromagnetic microwave absorption. *Compos. Part B* **2019**, *179*, 107417. [[CrossRef](#)]
45. Zhang, X.; Jia, Z.; Zhang, F.; Xia, Z.; Zou, J.; Gu, Z.; Wu, G. MOF-derived NiFe<sub>2</sub>S<sub>4</sub>/porous carbon composites as electromagnetic wave absorber. *J. Colloid Inter. Sci.* **2022**, *610*, 610–620. [[CrossRef](#)]
46. Wang, C.; Jia, Z.; He, S.; Zhou, J.; Zhang, S.; Tian, M.; Wang, B.; Wu, G. Metal-organic framework-derived CoSn/NC nanocubes as absorbers for electromagnetic wave attenuation. *J. Mater. Sci. Technol.* **2022**, *108*, 236–243. [[CrossRef](#)]
47. Qin, M.; Zhang, L.; Wu, H. Dual-template hydrothermal synthesis of multi-channel porous NiCo<sub>2</sub>O<sub>4</sub> hollow spheres as high-performance electromagnetic wave absorber. *Appl. Surf. Sci.* **2020**, *515*, 146132. [[CrossRef](#)]
48. Wu, L.; Wu, F.; Sun, Q.; Shi, J.; Xie, A.; Zhu, X.; Dong, W. A TTF–TCNQ complex: An organic charge-transfer system with extraordinary electromagnetic response behavior. *J. Mater. Chem. C* **2021**, *9*, 3316–3323. [[CrossRef](#)]
49. Wu, L.; Zhang, K.; Shi, J.; Wu, F.; Zhu, X.; Dong, W.; Xie, A. Metal/nitrogen co-doped hollow carbon nanorods derived from self-assembly organic nanostructure for wide bandwidth electromagnetic wave absorption. *Compos. Part B* **2022**, *228*, 109424. [[CrossRef](#)]
50. Lan, D.; Zhao, Z.; Gao, Z.; Kou, K.; Wu, H. Novel magnetic silicate composite for lightweight and efficient electromagnetic wave absorption. *J. Mater. Sci. Technol.* **2021**, *92*, 51–59. [[CrossRef](#)]
51. Zhao, H.; Cheng, Y.; Ma, J.; Zhang, Y.; Jia, G.; Du, Y. A sustainable route from biomass cotton to construct lightweight and high-performance microwave absorber. *Chem. Eng. J.* **2018**, *339*, 432–441. [[CrossRef](#)]
52. Shu, R.; Li, W.; Zhou, X.; Tian, D.; Zhang, G.; Gan, Y.; Shi, J.; He, J. Facile preparation and microwave absorption properties of RGO/MWCNTs/ZnFe<sub>2</sub>O<sub>4</sub> hybrid nanocomposites. *J. Alloy. Compd.* **2018**, *743*, 163–174. [[CrossRef](#)]